International Journal of Solids and Structures 49 (2012) 3762–3773

Contents lists available at SciVerse ScienceDirect

International Journal of Solids and Structures

journal homepage: www.elsevier.com/locate/ijsolstr

Non-linear buckling and postbuckling analysis of arches with unequal rotational end restraints under a central concentrated load

Yong-Lin Pi *, Mark Andrew Bradford

Centre for Infrastructure Engineering and Safety, School of Civil and Environmental Engineering, The University of New South Wales (UNSW), Sydney, NSW 2052, Australia

ARTICLE INFO

Article history:
Received 25 May 2012
Received in revised form 9 August 2012
Available online 23 August 2012

Keywords:
Analytical solution
Arches
Buckling
Elastic
Instability
Limit point
Non-linear
Restraints
Rotational
Relative flexibility
Unequal stiffness
Shallow

ABSTRACT

This paper presents an analytical study of the non-linear elastic in-plane buckling and postbuckling behaviour of pin-ended shallow circular arches having unequal elastic rotational end restraints under a central concentrated radial load. The principle of stationary potential energy is used to derive the differential equations of equilibrium, based on which the analytical solution for the non-linear equilibrium path is derived. It is found that the non-linear behaviour of an arch having unequal rotational end restraints is much more complicated than that of an arch with equal rotational end restraints. The arch may have a non-linear equilibrium path that consists of one or two unstable equilibrium paths and two or four limit points, and it may even have a non-linear looped equilibrium path in some cases. The number of limit points on the non-linear equilibrium path of an arch depends on its slenderness ratio and included angle, and on the stiffnesses of the unequal rotational end restraints. The switches in terms of an arch geometry parameter, which is introduced in the paper, are derived for distinguishing between arches with two limit points and those with four limit points, as well as for distinguishing between arches and beams curved in-elevation. The principle of conservation of energy at neutral equilibrium is used to derive the differential equations of buckling equilibrium, which are then used to investigate the buckling behaviour. It is found that an arch with unequal rotational end restraints cannot buckle in a bifurcation mode. Comparisons with finite element results show that the analytical solutions can accurately predict the non-linear buckling and postbuckling behaviour.

1. Introduction

It is known that an arch that is fully braced laterally and that is subjected to in-plane loading (Fig. 1) may buckle in its plane of loading. Analytical studies of the in-plane buckling of arches have been carried out by a number of researchers including Timoshenko and Gere (1961), Simitses (1976), Gjelsvik and Bodner (1962), Schreyer and Masur (1966), Dickie and Broughton (1971), Hodges (1999), Pi et al. (2002), Bradford et al. (2002) and Simitses and Hodges (2006). It has been found that the structural behaviour of a shallow arch becomes quite non-linear before in-plane buckling, and so the effects of this non-linearity on its in-plane buckling and postbuckling need to be considered. The non-linearity and instability of long panels with shallow arch cross-sections were investigated by Kyriakides and Arseculeratne (1993) and Power and Kyriakides (1994). Kyriakides and Arseculeratne (1993) addressed propagating buckling of long panels with shallow arch cross-sections, while Power and Kyriakides (1994) studied the response of long shallow elastic panels to uniform pressure loading. These panel studies considered a state of plane strain, and it was demonstrated that their response has the non-linearity and instabilities that are characteristic of shallow arches. Pi et al. (2002) studied the in-plane non-linear buckling of circular arches having an arbitrary uniform cross-section that are subjected to a radial load distributed uniformly around the arch axis, while Bradford et al. (2002) investigated the in-plane non-linear buckling of shallow circular arches of arbitrary cross-section that are subjected to a central concentrated radial load. Pi et al. (2007) investigated the in-plane non-linear elastic behaviour and stability of elastically supported shallow circular arches that are subjected to a radial load uniformly distributed around the arch axis. Pi et al. (2008) investigated the non-linear in-plane analysis and buckling of arches with elastic rotational end restraints under a central concentrated load, while Pi and Bradford (2009) derived analytical solutions for the non-linear postbuckling of these arches under uniform radial loading. These investigations were focused on arches having symmetrical boundary conditions.

In many cases, however, the ends of an arch are not restrained symmetrically. The unsymmetrical restraints and supports participate in the responses of an arch to external loading and they may influence significantly its in-plane buckling and postbuckling

* Corresponding author. Tel.: +61 2 9385 5094; fax: +61 2 9385 9747.
E-mail address: y.pi@unsw.edu.au (Y.-L. Pi).

0020-7683/$ - see front matter © 2012 Elsevier Ltd. All rights reserved.
http://dx.doi.org/10.1016/j.ijsolstr.2012.08.012

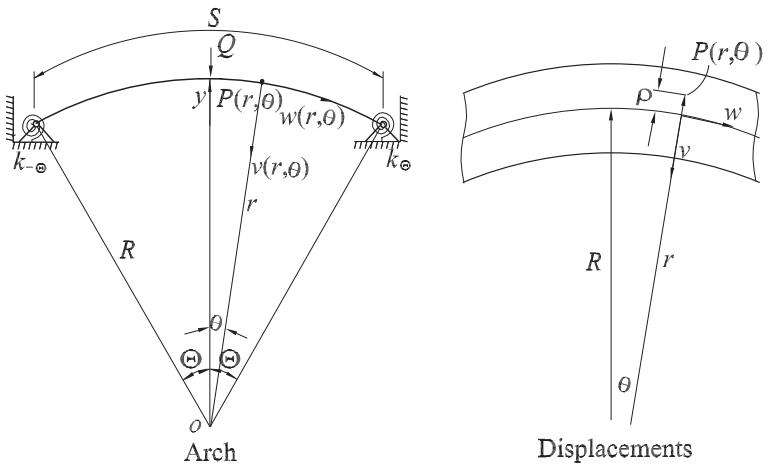

Fig. 1. Pin-ended arch with unequal rotational end restraints.

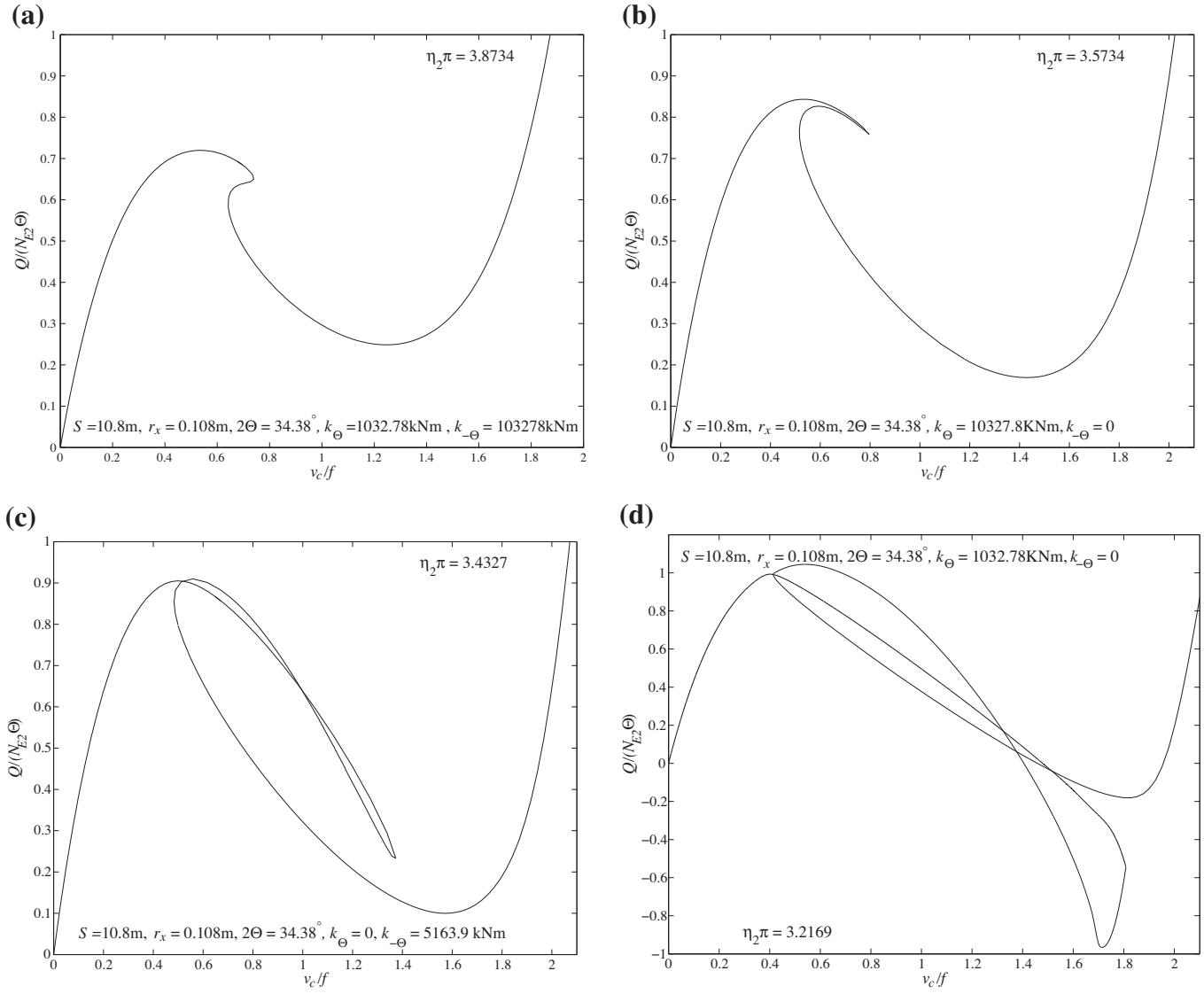

Fig. 2. FE results for arches with unequal rotational end restraints.

behaviour as shown by the finite element (FE) results of the beam element B21 of ABAQUS (2008) in Figs. 2(a)–(d) for the non-linear behaviour of an arch with unequal rotational end restraints under a central concentrated load, as variations of the dimensionless central radial displacement v_c/f with the dimensionless central concentrated load $Q/(N_{E2}\Theta)$, where Q is the central concentrated

load, N_{E2} is the second mode flexural buckling load of a column with the same length and boundary conditions as the arch, v_c is the central radial displacement, and f is the rise of the corresponding arch. It can be seen that the non-linear behaviour is very complicated and interesting.

This paper presents an investigation of the non-linear elastic in-plane behaviour and buckling of shallow circular pin-ended arches with unequal rotational end restraints under a central concentrated radial load. It provides a quantitative description of the highly complex and interesting behaviour.

2. Non-linear in-plane equilibrium

2.1. Differential equations of equilibrium

The polar coordinate system $oy\theta$ defined in Fig. 1 is used to describe the deformations of the arch. It has been shown (Pi et al., 2002; Bradford et al., 2002; Pi et al., 2008) that for shallow arches, the effects of axial deformations on the radial deformations and on the change of curvature are so small that neglecting these effects does not affect the non-linear analysis of shallow arches. Hence, the non-linear longitudinal normal stress and strain at an arbitrary point P (Fig. 1) can be written as

$$\sigma = E\epsilon \quad \text{and} \quad \epsilon = \epsilon_m + \epsilon_b \quad \text{with} \quad \epsilon_m = \tilde{w}' - \tilde{v} + \frac{1}{2}(\tilde{v}')^2 \quad \text{and} \quad \epsilon_b = -\frac{\rho\tilde{v}''}{R}, \tag{1}$$

where E is Young's modulus, ϵ_m and ϵ_b are the membrane and bending strains respectively; $()' \equiv \mathrm{d}()/\mathrm{d}\theta$, θ is the angular coordinate; $\tilde{v} = v/R$, $\tilde{w} = w/R$, v and w are the radial and axial displacements respectively, R is the radius of initial curvature of the arch, $\rho = r - R$, and r is the distance of the point P to the pole o of the axes $oy\theta$ (Fig. 1).

The total potential energy can expressed as

$$W = \frac{1}{2}\int_{-\Theta}^{\Theta}\int_A R\sigma\epsilon \mathrm{d}A\mathrm{d}\theta - \int_{-\Theta}^{\Theta}\mathrm{Dirac}(\theta)QR\tilde{v}\mathrm{d}\theta + \frac{1}{2}\sum_{i=\pm\Theta} k_i\tilde{v}_i^2, \tag{2}$$

where $k_i (i = \pm\Theta)$ is the stiffness of the rotational end restraints, and $\mathrm{Dirac}(\theta)$ is the familiar Dirac-delta function defined by

$$\mathrm{Dirac}(\theta) = \begin{cases} +\infty, & \theta = 0 \\ 0, & \theta \neq 0 \end{cases} \quad \text{and} \quad \int_{-\infty}^{\infty}\mathrm{Dirac}(\theta)\mathrm{d}\theta = 1 \tag{3}$$

and it has the property

$$\int_{-\infty}^{\infty}\mathrm{Dirac}(\theta)f(\theta)\mathrm{d}\theta = f(0). \tag{4}$$

The differential equations of equilibrium can be derived from Eq. (2) by substituting Eq. (1) into it and applying the principle of stationary potential energy as

$$(NR)' = 0 \quad \text{and} \quad \frac{\tilde{v}^{iv}}{\mu^2} + \tilde{v}'' = \frac{QR^2\mathrm{Dirac}(\theta)}{\mu^2 EI_x} - 1 \quad \text{with} \quad \mu^2 = \frac{NR^2}{EI_x} \tag{5}$$

for the axial and radial deformations respectively, where μ is a dimensionless axial force parameter, I_x is the in-plane second moment of area and N is the axial compressive force given by

$$N = -AE\epsilon_m = -AE\left(\tilde{w}' - \tilde{v} + \frac{1}{2}\tilde{v}'^2\right) \tag{6}$$

with A being the cross-sectional area.

The static boundary conditions can also obtained in the same way as

$$2\Theta\alpha_i\tilde{v}_i'' \pm \tilde{v}_i' = 0 \quad \text{with} \quad i = \pm\Theta, \tag{7}$$

where $\alpha_i = EI/k_iS$ is the ratio of the bending stiffness per unit length of the arch (EI/S) to k_i, which can be considered as the relative flexibility of the elastic rotational end restraints.

In addition, the essential kinematic boundary conditions are

$$\tilde{v} = 0 \quad \text{and} \quad \tilde{w} = 0 \quad \text{at} \quad \theta = \pm\Theta. \tag{8}$$

The dimensionless radial displacement $\tilde{v}$, which satisfies the boundary conditions given by Eqs. (7) and (8), can be obtained by solving the differential equation of equilibrium given by Eq. (5) as

$$\tilde{v} = \frac{1}{\mu^2}\left\{K_1\beta(\cos\mu\theta - \cos\beta) + K_2(\beta\sin\mu\theta - \mu\theta\sin\beta) + \frac{1}{2}[\beta^2 - (\mu\theta)^2]\right\} + \frac{P}{\mu^2\beta}\{K_3(\beta\sin\mu\theta - \mu\theta\sin\beta) + K_4\cos\mu\theta + K_5 - \beta + H(\theta)(\mu\theta - \sin\mu\theta)\}, \tag{9}$$

where β is a new dimensionless axial force parameter and P is the dimensionless central load defined as

$$\beta = \mu\Theta \quad \text{and} \quad P = \frac{QR^2\Theta}{2EI_x\mu}, \tag{10}$$

respectively, the parameters K_1, K_2, K_3, and K_4 are given by

$$K_1 = \frac{\Psi_1}{\Phi}, \quad K_2 = \frac{\Psi_2}{\Phi}, \quad K_3 = \frac{\Psi_3}{\Phi}, \quad K_4 = \frac{\Psi_4 + \Psi_5}{\Phi}, \quad K_5 = \frac{\Psi_4 - \beta\sin^2\beta}{\Phi}, \tag{11}$$

with

$$\Phi = \sin^2\beta + \beta(\cos\beta\sin\beta - \beta\cos 2\beta)(\alpha_\Theta + \alpha_{-\Theta}) + (4\beta^2\alpha_\Theta\alpha_{-\Theta} - 1)\beta\sin\beta\cos\beta, \tag{12}$$

$$\Psi_1 = [\beta\cos\beta - (1 + \beta^2)\sin\beta](\alpha_\Theta + \alpha_{-\Theta}) - (4\beta^2\alpha_\Theta\alpha_{-\Theta} + 1) \times \sin\beta + \beta\cos\beta, \tag{13}$$

$$\Psi_2 = \beta(\beta\cos\beta - \sin\beta)(\alpha_\Theta - \alpha_{-\Theta}), \quad \Psi_3 = \beta(1 - \cos\beta)(\alpha_\Theta - \alpha_{-\Theta}), \tag{14}$$

$$\Psi_4 = \beta^2\sin\beta(1 - \cos\beta)(\alpha_\Theta + \alpha_{-\Theta}) + (\beta + \sin\beta)(1 - \cos\beta), \tag{15}$$

$$\Psi_5 = \beta\sin^2\beta(4\beta^2\alpha_\Theta\alpha_{-\Theta} - 1) + \beta\sin\beta(\alpha_\Theta + \alpha_{-\Theta})(\sin\beta - \beta\cos\beta) \tag{16}$$

and the step function $H(\theta)$ is modified from the familiar Heaviside function as

$$H(\theta) = [2 \times \mathrm{Heaviside}(\theta) - 1] \quad \text{with} \quad \mathrm{Heaviside}(\theta) = \begin{cases} 0 & \theta < 0 \\ \text{undefined} & \theta = 0 \\ 1 & \theta > 0 \end{cases}. \tag{17}$$

It is noted that although the function $\mathrm{Heaviside}(\theta)$ given in Eq. (17) is undefined at $\theta = 0$, the term $\mathrm{Heaviside}(\theta)[\mu\theta - \sin(\mu\theta)]$ in the radial displacement expression given by Eq. (9) vanishes at $\theta = 0$ and so the displacement $\tilde{v}$ given by Eq. (9) is also defined at $\theta = 0$.

2.2. Non-linear equilibrium equation

From Eq. (9), it can be seen that the radial displacement is a function of the central concentrated load Q and the internal axial compressive force N. To evaluate the radial displacement, a non-linear relationship between the axial compressive force and the external load needs to be derived. From the first of Eq. (5), the axial compressive force N in the arch is a constant. The non-linear relationship between the central concentrated load Q and the axial compressive force N can be established by considering that the

constant axial force is equal to the axial force averaged mathematically over the arch length domain calculated from Eq. (6) as

$$N = -\frac{1}{2\Theta}\int_{-\Theta}^{\Theta} AE\left(\tilde{w}' - \tilde{v} + \frac{\tilde{v}'^2}{2}\right)\mathrm{d}\theta. \tag{18}$$

Considering the boundary condition given by Eq. (8), and substituting Eq. (9) into Eq. (18) and then integrating Eq. (18) leads to the non-linear equilibrium equation between the central concentrated load Q (through P) and the internal axial force N (through β) as the transcendental equation

$$A_1P^2 + B_1P + C_1 = 0, \tag{19}$$

where the coefficients A_1, B_1 and C_1 are given by

$$A_1 = \Xi_1K_4^2 - \Xi_2K_4 + \Xi_3K_3^2 + \Xi_4, \tag{20}$$

$$B_1 = 2\beta^2\Xi_1K_1K_4 - \beta^2\Xi_2K_1 + 2\beta\Xi_3K_2K_3 - \frac{\cos\beta K_4}{\beta^3} + \frac{\sin\beta - K_5}{\beta^3}, \tag{21}$$

$$C_1 = \left(\frac{\beta}{\lambda}\right)^2 + \beta^4\Xi_1K_1^2 + \beta^2\Xi_3K_2^2 - \frac{1}{6} \quad \text{with} \quad \lambda = \frac{R\Theta^2}{r_x} = \frac{S\Theta}{2r_x} \tag{22}$$

in which λ is the geometric parameter for the arch, r_x is the major axis radius of gyration and the parameters Ξ_1, Ξ_2, Ξ_3, and Ξ_4 are given by

$$\Xi_1 = \frac{\beta - \cos\beta\sin\beta}{4\beta^5}, \quad \Xi_2 = \frac{(\cos\beta - 1)^2}{2\beta^5}, \tag{23}$$

$$\Xi_3 = \frac{\beta\cos\beta\sin\beta + \beta^2 - 2\sin^2\beta}{4\beta^4},$$
$$\Xi_4 = \frac{\cos\beta\sin\beta + 3\beta - 4\sin\beta}{4\beta^5}. \tag{24}$$

When the geometry of an arch and the stiffness of the rotational end restraints are given, its geometric parameter λ and the relative flexibility α_i ($i = \pm\Theta$) of the rotational end restraints are defined. Eq. (19) can then be used to derive the variations of the dimensionless force parameter β with the dimensionless central load P. Subsequently, substituting the obtained values of β and P into Eq. (9) leads to the variations of the radial displacement $\tilde{v}$ with the dimensionless central load P.

The typical non-linear behaviour of pin-ended arches with unequal rotational end restraints is shown in Fig. 3 as variations of

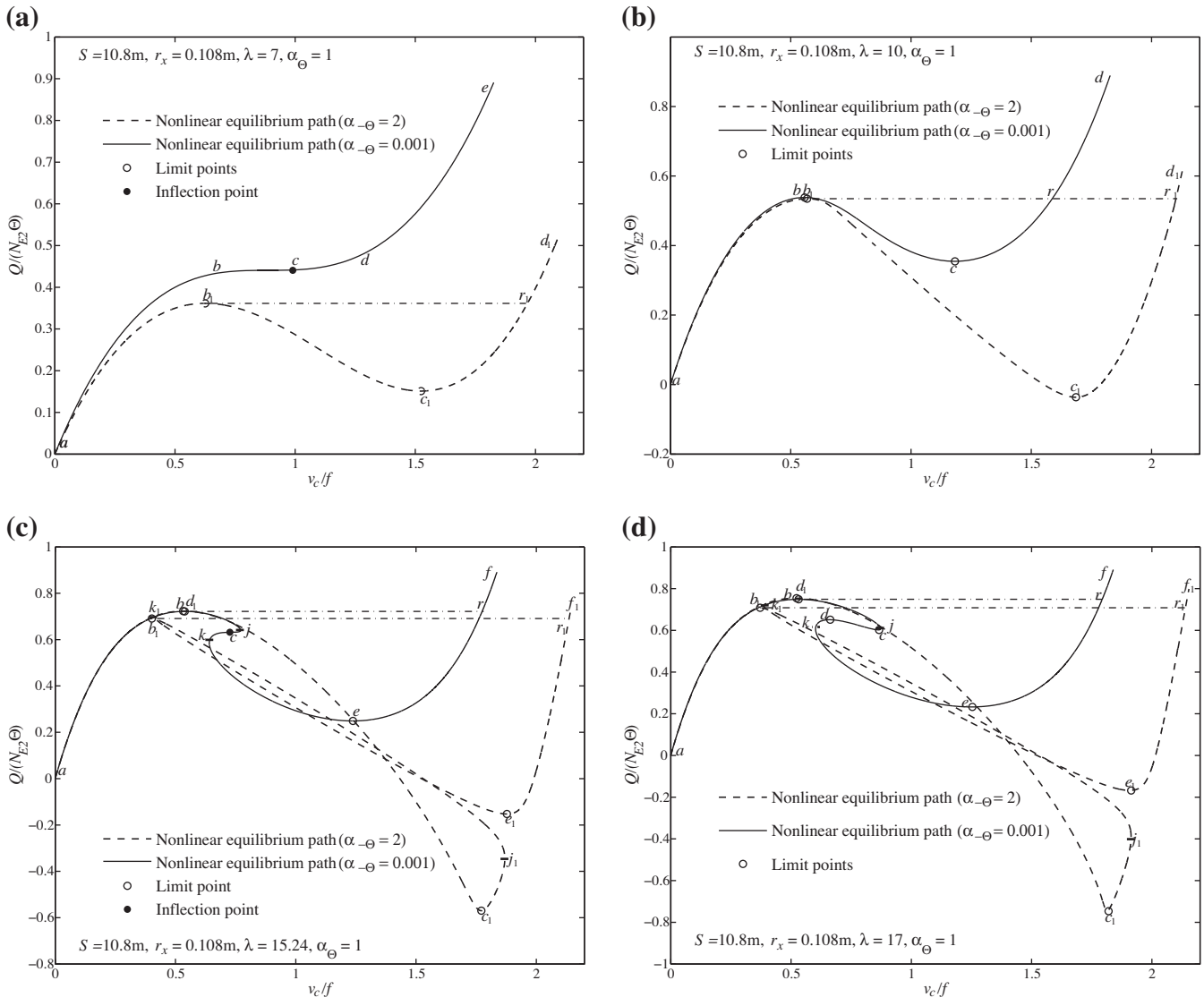

Fig. 3. Non-linear equilibrium path for arches.

the dimensionless central displacement v_c/f with the dimensionless central concentrated load $Q/(N_{E2}\Theta)$ for two groups of arches: one with $\alpha_\Theta = 1$ and $\alpha_{-\Theta} = 0.001$ (solid curve) and the other with $\alpha_\Theta = 1$ and $\alpha_{-\Theta} = 2$ (dashed curve), where for the convenience of comparison, N_{E2} is the second mode flexural buckling load of a column with the same length and boundary conditions as those of the arches with $\alpha_\Theta = 1$ and $\alpha_{-\Theta} = 0.001$. It can be seen that for the arch with $\lambda = 7$ (Fig. 3(a)), when $\alpha_{-\Theta} = 0.001$ (solid curve), there are two stable equilibrium branches *ab* and *de*, and the equilibrium path *bcd* with a nearly zero slope with an inflection point *c*. At the branch *bcd*, the dimensionless displacement v_c/f increases significantly with little increase of the dimensionless load $Q/(N_{E2}\Theta)$. When $\alpha_{-\Theta} = 2$ (dashed curve), there are two stable equilibrium branches ab_1 and c_1d_1, an unstable equilibrium branch b_1c_1 and an upper limit point b_1 and a lower limit point c_1. In the unstable equilibrium branch b_1c_1, the increase of the dimensionless displacement v_c/f is associated with a decrease of the dimensionless load $Q/(N_{E2}\Theta)$ until lower limit point c_1 is reached. For the arch with $\lambda = 10$ (Fig. 3(b)), when $\alpha_{-\Theta} = 0.001$ (solid curve), its equilibrium behaviour is similar to that of the arch with $\lambda = 7$ and $\alpha_{-\Theta} = 2$ (dashed curve in Fig. 3(a)). When $\alpha_{-\Theta} = 2$, the unstable equilibrium path b_1c_1 is longer than that when $\alpha_{-\Theta} = 0.001$. In addition, the lower limit point load is negative when $\alpha_{-\Theta} = 2$, while it is positive when $\alpha_{-\Theta} = 0.001$.

The non-linear behaviour of the arches with $\lambda = 15.24$ and $\lambda = 17$ in Fig. 3(c) and (d) is much more complicated. For the arch with $\lambda = 15.24$ (Fig. 3(c)), when $\alpha_{-\Theta} = 0.001$ (solid curve), its equilibrium path includes an upper limit point *b*, an inflection point *c*, and a lower limit point *d*, three stable equilibrium branches *ab*, *jk*, and *ef* with a positive slope, and two unstable branches *bj* and *ke*. At the points *j* and *k*, there is a vertical tangent (implying $dv_c/dQ = 0$). The inflection point *c* is located at the reverse segment *jk*. The upper limit point buckling load, lower limit point load and the load at the inflection point are all positive. When $\alpha_{-\Theta} = 2$ (dashed curve), the non-linear equilibrium path of the arch is completely different and it consists of two upper limit points b_1 and d_1, two lower limit points c_1 and e_1, four stable equilibrium branches ab_1, j_1c_1, d_1k_1, e_1f_1 with a positive slope, and three unstable equilibrium branches b_1j_1, c_1d_1, k_1e_1 with a negative slope. In addition, the two lower limit point buckling loads are negative while the two upper limit point buckling loads are positive. Furthermore, the arch has a very complicated non-linear looped equilibrium path. The second upper limit point when $\alpha_{-\Theta} = 2$ almost coincides with the upper limit point when $\alpha_{-\Theta} = 0.001$.

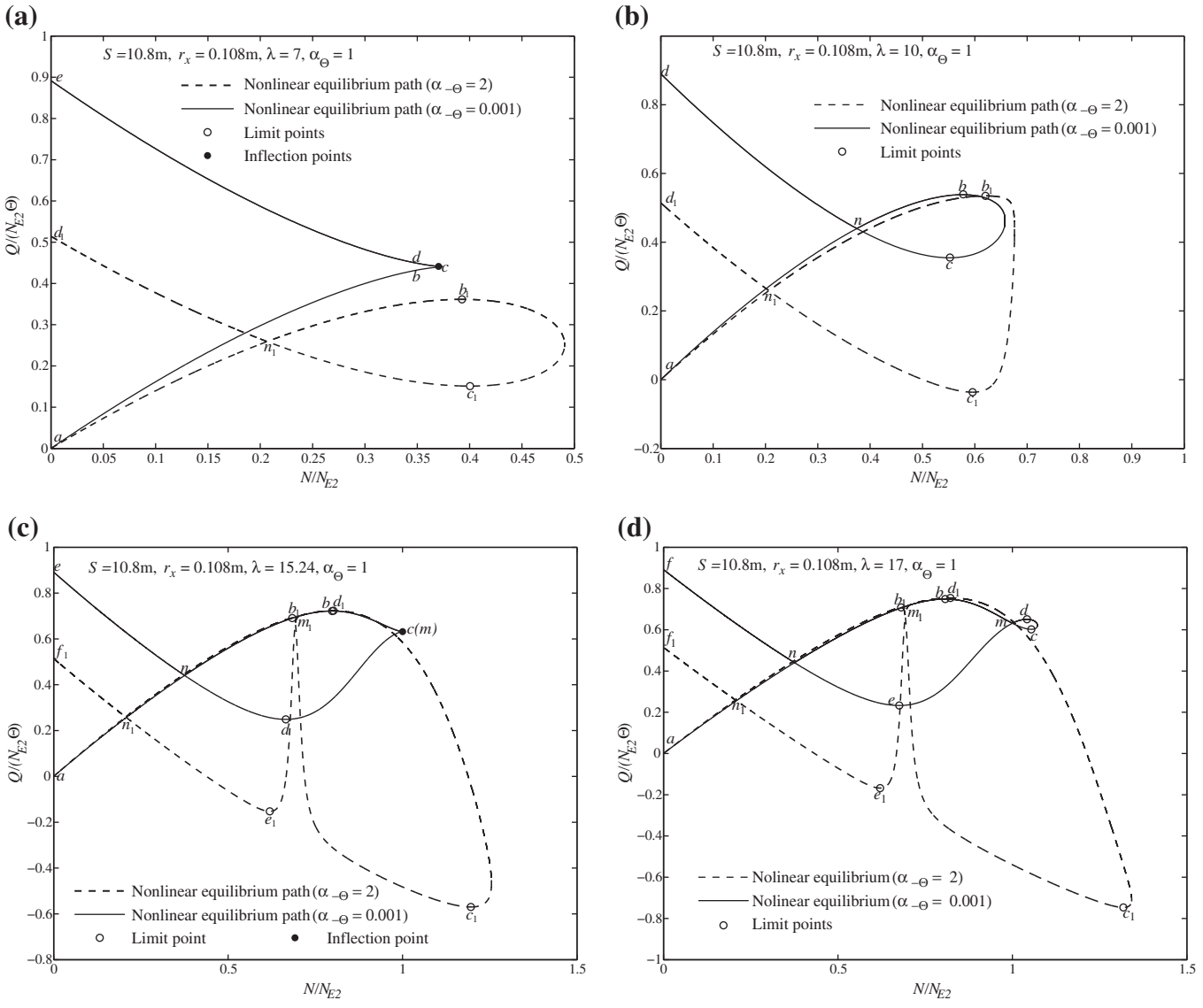

Fig. 4. Non-linear equilibrium between axial force and central load for arches.

For the arch with $\lambda = 17$ (Fig. 3(d)), when $\alpha_{-\Theta} = 0.001$ (solid curve) and $\alpha_{-\Theta} = 2$ (dashed curve), the non-linear equilibrium path has two upper limit points b (b_1) and d (d_1), two lower limit points c (c_1) and e (e_1), four stable equilibrium branches ab (ab_1), jc (j_1c_1), dk (d_1k_1), and ef (e_1f_1), and three unstable equilibrium branches bj (b_1j_1), cd (c_1d_1), ke (k_1e_1) with a negative slope, where the subscript 1 is for the case of $\alpha_{-\Theta} = 2$. In addition, the arch with $\alpha_{-\Theta} = 2$ has a very complicated non-linear looped equilibrium path. For $\alpha_{-\Theta} = 0.001$, the two upper limit point and two lower limit point buckling loads are all positive, while for $\alpha_{-\Theta} = 2$, the two lower limit point buckling loads are negative and the two upper limit point buckling loads are positive. The second upper limit point for $\alpha_{-\Theta} = 2$ almost coincides with the first limit point for $\alpha_{-\Theta} = 0.001$.

The non-linear behaviour of these two arches is also illustrated in Fig. 4 as variations of the dimensionless axial force N/N_{E2} with the dimensionless central concentrated load $Q/(N_{E2}\Theta)$. It can also be seen that the relative flexibility of the end rotational restraints has a significant effect on the non-linear behaviour. The arch with more flexible end rotational restraints ($\alpha_{-\Theta} = 2$) (dashed curve) has more complicated non-linear behaviour than that of the arch with more stiff end rotational restraints ($\alpha_{-\Theta} = 0.001$) (solid curve). It can also be seen that the dimensionless axial force-load curve is self intersecting at the point n (n_1) for the arch geometric parameter $\lambda = 7$ and $\lambda = 10$ or n and m (n_1 and m_1) for $\lambda = 15.24$ and $\lambda = 17$. For the case of $\alpha_{-\Theta} = 0.001$, the point n for the arch with $\lambda = 7$ corresponds to the maximum axial compressive force (Fig. 4(a)), while the point m for the arch with $\lambda = 15.24$ corresponds to the maximum axial compressive force (Fig. 4(c)).

In summary, the relative flexibilities of unequal rotational end restraints α_{Θ} and $\alpha_{-\Theta}$ and the arch geometric parameter λ have significant effects on the non-linear buckling and postbuckling behaviour of an arch. They affect not only the limit point buckling load and the number of the limit points, but also the shape of the non-linear equilibrium path and the number of different equilibrium branches of the arch.

2.3. Limit points

Since the upper and lower limit points represent relative maxima and minima, they can be derived using routine calculus in conjunction with the definitions of μ in Eq. (5) and with Eqs. (10) and (19). For this, the central load Q can be expressed as an implicit function of the dimensionless axial force parameter β as $F(Q,\beta) = 0$, and the loads corresponding to the upper and lower limit points can be obtained by setting $\mathrm{d}Q/\mathrm{d}\beta = -[\partial F(Q,\beta)/\partial\beta]/[\partial F(Q,\beta)/\partial Q] = 0$, which leads to the non-linear equation of equilibrium between the dimensionless load P and the axial force parameter β at the limit points as the transcendental equation

$$A_2P^2 + B_2P + C_2 = 0, \tag{25}$$

where the coefficients A_2, B_2 and C_2 are given by

$$A_2 = \left(\frac{5}{2}\Xi_1 - \frac{\sin^2\beta}{4\beta^4}\right)K_4^2 - \left(\frac{5}{2}\Xi_2 - \Xi_5\right)K_4 + (2\Xi_3 - \Xi_6)K_3^2 - \beta\Xi_1K_4\frac{\mathrm{d}K_4}{\mathrm{d}\beta} + \frac{\beta\Xi_2}{2}\frac{\mathrm{d}K_4}{\mathrm{d}\beta} - \beta\Xi_3K_3\frac{\mathrm{d}K_3}{\mathrm{d}\beta} + \frac{5}{2}\Xi_4 - \Xi_7, \tag{26}$$

$$B_2 = \left(3\beta^2\Xi_1 - \frac{\sin^2\beta}{2\beta^2}\right)K_1K_4 - \beta^2\left(\frac{3}{2}\Xi_2 - \Xi_5\right)K_1 + (3\beta\Xi_3 - 2\beta\Xi_6)K_2K_3 - \left(\frac{\sin\beta}{2\beta^2} + \frac{3\cos\beta}{2\beta^3}\right)K_4 - \frac{3K_5}{2\beta^3} + \frac{3\sin\beta}{2\beta^3} - \frac{\cos\beta}{2\beta^2} - \beta^3\Xi_1\frac{\mathrm{d}K_1K_4}{\mathrm{d}\beta} + \frac{\beta^3\Xi_2}{2}\frac{\mathrm{d}K_1}{\mathrm{d}\beta} - \beta^2\Xi_3\frac{\mathrm{d}K_2K_3}{\mathrm{d}\beta} + \frac{\cos\beta}{2\beta}\frac{\mathrm{d}K_4}{\mathrm{d}\beta} + \frac{\mathrm{d}K_5}{2\beta^2\mathrm{d}\beta}, \tag{27}$$

$$C_2 = \left(\frac{\beta^4}{2}\Xi_1 - \frac{\sin^2\beta}{4}\right)K_1^2 + (\beta^2\Xi_3 - \beta^2\Xi_6)K_2^2 - \beta^5\Xi_1K_1\frac{\mathrm{d}K_1}{\mathrm{d}\beta} - \beta^3\Xi_3K_2\frac{\mathrm{d}K_2}{\mathrm{d}\beta} - \left(\frac{\beta}{\lambda}\right)^2, \tag{28}$$

with

$$\Xi_5 = \frac{1 - \cos\beta\sin\beta}{2\beta^4}, \quad \Xi_6 = \frac{2\beta + \beta\cos 2\beta - 3\cos\beta\sin\beta}{8\beta^3}, \quad \text{and} \quad \Xi_7 = \frac{\cos 2\beta + 3 - 4\cos\beta}{8\beta^4}. \tag{29}$$

The analytical solutions for the limit buckling load P and the corresponding axial force parameters β at the limit buckling points can be obtained by solving Eqs. (19) and (25) simultaneously. The corresponding radial displacement $\tilde{v}$ can then be obtained from Eq. (9).

The solutions for the limit buckling load, the corresponding axial forces and central radial displacement were obtained and are shown by circles for the arches in Figs. 3 and 4.

3. Non-linear bifurcation buckling analysis

In addition to the limit point buckling, arches with symmetric boundary conditions may also buckle in a bifurcation mode (Pi et al., 2002; Pi and Bradford, 2009, 2010). An investigation is undertaken in this section to ascertain whether an arch with unequal rotational end restraints can buckle in a bifurcation mode as well.

The bifurcation point of a structural system is a stationary point, at which the equilibrium state of the system is neutral (Simitses and Hodges, 2006). Conservation of energy at neutral equilibrium requires that second variation of the total potential energy vanishes at the stationary points (Bažant and Cedolin, 2003) as $\delta^2W = 0$. Substituting the total potential energy given by Eq. (2) into the second variation of the total potential energy and integrating it by parts leads to the differential equations of buckling equilibrium as (Pi and Bradford, 2012)

$$AER\epsilon'_{mb} = 0 \quad \text{and} \quad \frac{EI}{R}\tilde{v}_b^{(iv)} + NR\tilde{v}''_b - AER\epsilon_{mb}(1 + \tilde{v}'') = 0 \tag{30}$$

in the axial and radial directions; and to the static boundary conditions as

$$2\Theta\alpha_{\Theta}\tilde{v}''_b + \tilde{v}'_b = 0 \quad \text{at} \quad \theta = \Theta \quad \text{and} \quad -2\Theta\alpha_{-\Theta}\tilde{v}''_b + \tilde{v}'_b = 0 \quad \text{at} \quad \theta = -\Theta. \tag{31}$$

In addition, the essential kinematic boundary conditions in the axial and radial directions are

$$\tilde{w}_b = 0 \quad \text{and} \quad \tilde{v}_b = 0 \quad \text{at} \quad \theta = \pm\Theta. \tag{32}$$

It is known that during bifurcation buckling, both the load and internal stress resultants remain unchanged, so that $N_b = \delta N = AE\epsilon_{mb} = 0$, from which the membrane strain produced by the buckling deformation vanishes as

$$\epsilon_{mb} = \tilde{w}'_b - \tilde{v}_b + \tilde{v}'\tilde{v}'_b = 0. \tag{33}$$

Substituting Eq. (33) into Eq. (30) leads to the differential equations for bifurcation buckling as

$$\frac{\tilde{v}_b^{iv}}{\mu^2} + \tilde{v}''_b = 0. \tag{34}$$

The equation given by Eq. (34) is a four order homogeneous differential equation and its solution has four undetermined coefficients,

which in conjunction with the boundary conditions given by Eqs. (31) and (32) forms an eigenvalue equation with the four undetermined coefficients. For the existence of nontrivial solutions of the coefficients, the characteristic equation

$$[2\alpha_\Theta\alpha_{-\Theta}\beta^2+(\alpha_\Theta+\alpha_{-\Theta}-1)/2]\beta\sin 2\beta-(\alpha_\Theta+\alpha_{-\Theta})\beta^2\cos 2\beta+\sin^2\beta=0 \tag{35}$$

needs to be satisfied, which can be used to investigate whether bifurcation buckling of pin-ended arches with unequal elastic rotational end restraints is possible.

When the values of the relative flexibility of the rotational end restraints α_Θ and $\alpha_{-\Theta}$ are given, the second lowest value of the parameter $\beta\,(=\mu\Theta)$ corresponding to possible bifurcation buckling can be evaluated from Eq. (35) as

$$\beta=\mu\Theta=\eta_2\pi\Rightarrow N=\frac{(\eta_2\pi)^2EI}{(S/2)^2}=N_{E2}. \tag{36}$$

However, although the values $\beta=\eta_2\pi$ of the dimensionless axial force parameter β can be obtained from Eq. (35) mathematically, the arch does not necessarily buckle in a bifurcation mode. To illustrate this, the zero membrane strain ϵ_{mb} during bifurcation buckling given by Eq. (33) can be expressed as

$$\epsilon_{mb}=\frac{1}{2\Theta}\int_{-\Theta}^{\Theta}(\tilde{w}_b'-\tilde{v}_b+\tilde{v}'\tilde{v}_b')\mathrm{d}\theta=\frac{1}{2\Theta}\left\{\int_{-\Theta}^{\Theta}\tilde{w}_b'\mathrm{d}\theta-\int_{-\Theta}^{\Theta}\tilde{v}_b\mathrm{d}\theta+\int_{-\Theta}^{\Theta}\tilde{v}'\tilde{v}_b'\mathrm{d}\theta\right\}=0. \tag{37}$$

If an arch is to buckle in a bifurcation buckling mode, the buckling radial displacements $\tilde{v}_b$ should be orthogonal to the corresponding primary displacements $\tilde{v}$, from which the last term of Eq. (37) vanishes as $\int_{-\Theta}^{\Theta}\tilde{v}'\tilde{v}_b'\mathrm{d}\theta=0$. In addition, the buckling axial displacements $\tilde{w}_b$ at both ends are equal to zero as given by Eq. (32) and so the first term of Eq. (37) also vanishes as $\int_{-\Theta}^{\Theta}\tilde{w}_b'\mathrm{d}\theta=0$. Hence, Eq. (37) would reduce to

$$\epsilon_{mb}=-\frac{1}{2\Theta}\int_{-\Theta}^{\Theta}\tilde{v}_b\mathrm{d}\theta=0, \tag{38}$$

which holds only when the buckling radial displacements $\tilde{v}_b$ are antisymmetric along the arch length. Hence, primary radial displacements $\tilde{v}$ that are orthogonal to the antisymmetric buckling radial displacements $\tilde{v}_b$ have to be symmetric. However, the radial displacement $\tilde{v}$ of an arch with unequal rotational end restraints given by Eq. (9) is unsymmetrical along the arch length. Typical radial displacement distributions along the arch length obtained from Eq. (9) are shown in Fig. 5(a) for an arch with a geometric parameter $\lambda=20$ and with $\alpha_\Theta=1$ and $\alpha_{-\Theta}=0.001$, and in Fig. 5(b) for the same arch but with $\alpha_\Theta=0.2$ and $\alpha_{-\Theta}=20$. It can be seen that the distributions of the displacements $\tilde{v}$ are unsymmetrical along the arch length. Hence, the possible orthogonal bifurcation buckling displacements $\tilde{v}_b$ cannot be antisymmetric along the arch length and its integral over the arch length, i.e. Eq. (38), does not vanish. Subsequently, the buckling strain ϵ_{mb} given by Eq. (37) and the variation of the axial force N_b do not vanish, and so bifurcation buckling of the arch cannot occur.

4. Switches between different non-linear behaviour

Although bifurcation buckling cannot occur, the solution $\beta=\eta_2\pi$ given by Eq. (36) defines an arch with a specific geometric parameter λ_2, which can serve as a switch to distinguish arches with two limit points and those with four limit points.

The dimensionless load P corresponding to the solution $\beta=\eta_2\pi$ can be solved from Eq. (19) as

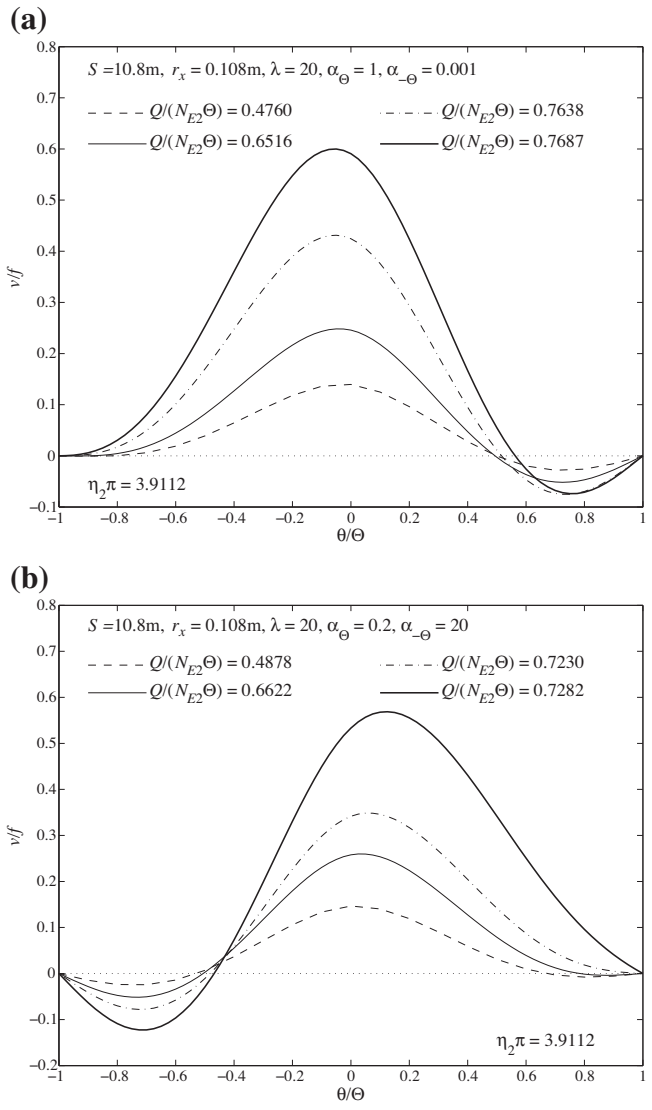

Fig. 5. Distributions of the radial displacement along the arch length.

$$P=\lim_{\beta\to\eta_2\pi}\left[-\frac{B_1}{2A_1}\pm\sqrt{\frac{B_1^2}{4A_1^2}-\frac{C_1}{A_1}}\right]\quad\text{with}\quad\frac{B_1^2}{4A_1^2}-\frac{C_1}{A_1}\geqslant 0. \tag{39}$$

Substituting the expression of C_1 given by Eq. (22) into the second equation of Eq. (39) leads to

$$\lambda_2=\lim_{\beta\to\eta_2\pi}\sqrt{\frac{4\beta^2A_1}{B_1^2-4A_1D_1}}, \tag{40}$$

where limit evaluation is used because A_1, B_1 and D_1 approach infinity when β approaches $\eta_2\pi$.

When the geometric parameter λ is equal to λ_2 given by Eq. (40), the expression in the radical of Eq. (39) vanishes and so the dimensionless load P corresponding to λ_2 given by Eq. (39) becomes

$$P=\lim_{\beta\to\eta_2\pi}(B_1/2A_1). \tag{41}$$

Hence, the arch with the specific geometric parameter λ_2 corresponds a unique solution for the dimensionless load P and dimensionless axial force parameter $\beta=\eta_2\pi$. Once the relative flexibilities α_Θ and $\alpha_{-\Theta}$ are given, the solution of $\beta=\eta_2\pi$ can be evaluated from Eq. (35) and then the specific geometric slenderness λ_2 can be obtained from Eq. (40). To demonstrate this, four groups of arches with different

rotational end restraints were investigated using the non-linear equation given by Eq. (19). The results are shown in Figs. 6 and 7 as variations of the dimensionless load $Q/(N_{E2}\Theta)$ with the dimensionless axial force N/N_{E2}. The rotational end restraints of the group in Figs. 6(a) and (b) and 7(a) and (b) have relative flexibilities $\alpha_\Theta = 2$ and $\alpha_{-\Theta} = 0.01$, $\alpha_\Theta = 1$ and $\alpha_{-\Theta} = 0$, $\alpha_\Theta = 1$ and $\alpha_{-\Theta} = 2$, and $\alpha_\Theta = 1$ and $\alpha_{-\Theta} = \infty$, respectively. The specific geometric parameters obtained from Eq. (40) are $\lambda_2 = 15.0644$, 15.239, 13.505, and 13.45 for the group of arches in Figs. 6(a) and (b) and 7(a) and (b), respectively. It can be seen from Fig. 6(a) and (b) that arches with a geometric parameter $\lambda = 10$, 12, and 14 that are smaller than λ_2 have an upper limit point and a lower limit point while arches with $\lambda = 20$, 25, 30 and 40 that are larger than λ_2 have two upper limit points and two lower limit points. In the same way, the arches in Fig. 7(a) and (b) with a geometric parameter $\lambda = 6$, 8, and 10 that are smaller than λ_2 have an upper limit point and a lower limit point while arches with $\lambda = 15$, 16, 20 and 40 that are larger than λ_2 have two upper limit points and two lower limit points.

When an arch is very flat, it is subjected mainly to bending action and has no typical buckling behaviour, and so can be treated a beam curved in elevation. To determine this, the arch that has a lowest buckling load needs to be identified. The axial force parameter β corresponding to the arch with the lowest buckling load can be derived from the lowest solution of Eq. (35) as

$$\beta = \eta_1\pi. \tag{42}$$

The dimensionless load P corresponding to the solution $\beta = \eta_1\pi$ can be solved from Eq. (19) as given by Eq. (39) by replacing $\lim_{\beta\to\eta_2\pi}$ with $\lim_{\beta\to\eta_1\pi}$, and the corresponding value of the arch geometric parameter λ_1 can also be obtained from Eq. (40) by replacing $\lim_{\beta\to\eta_2\pi}$ with $\lim_{\beta\to\eta_1\pi}$.

When the geometric parameter λ is equal to λ_1, the expression in the radical of Eq. (39) vanishes and so the dimensionless load P corresponding to λ_1 can be obtained from Eq. (41) by replacing $\lim_{\beta\to\eta_2\pi}$ with $\lim_{\beta\to\eta_1\pi}$. When the relative flexibilities of elastic rotational end restraints are given, the lowest solution of $\beta = \eta_1\pi$ can be evaluated from the characteristic equation given by Eq. (35). The corresponding dimensionless radial displacement $\tilde{v}$, specific geometric parameter λ_1, and dimensionless central load P can be calculated from (9), (40), and (41) by replacing $\lim_{\beta\to\eta_2\pi}$ with $\lim_{\beta\to\eta_1\pi}$. For example, typical non-linear behaviour of the arch with $\alpha_\Theta = 1$, $\alpha_{-\Theta} = 0.001$, and the geometric parameter $\lambda_1 = 7$ was shown in Fig. 3(a) as variations of the dimensionless central radial displacement v_c/f with the dimensionless load $Q/(N_{E2}\Theta)$, and in Fig. 4(a) as variation of the dimensionless axial force N/N_{E2} with the dimensionless load $Q/(N_{E2}\Theta)$. It can be evaluated that $\beta = \eta_1\pi = 2.394$, $\lambda_1 = 7$, and $P = 3.3638$. The central radial displacement corresponding to the inflection point c in Fig. 3(a)

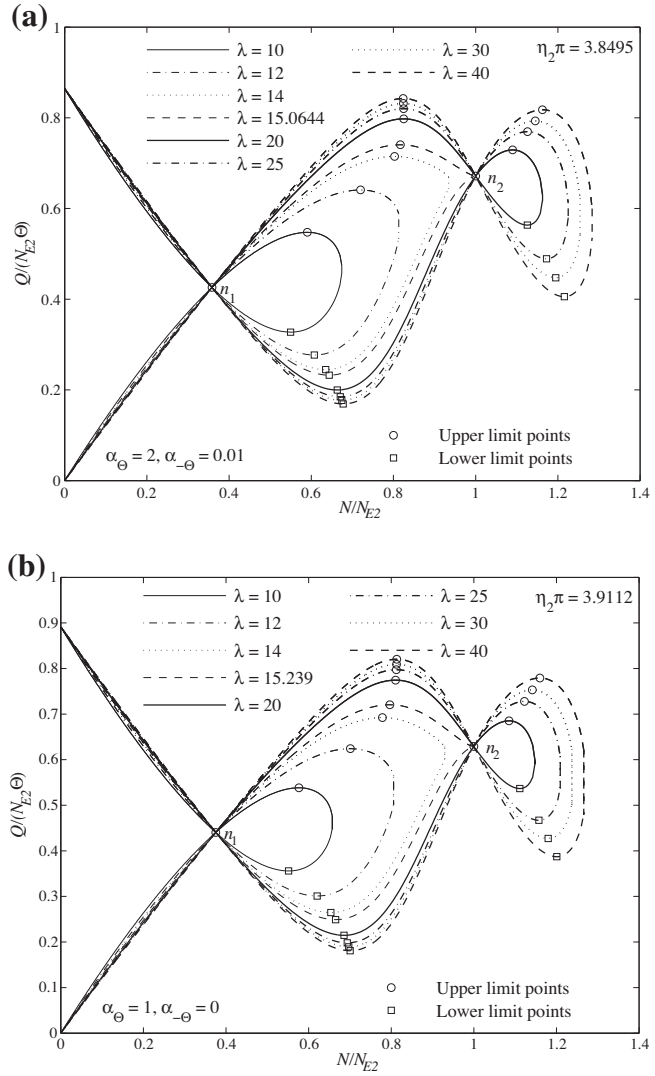

Fig. 6. Non-linear relationship of axial force with central load for arches with $\alpha_\Theta = 2$ and $\alpha_{-\Theta} = 0.01$ or $\alpha_\Theta = 1$ and $\alpha_{-\Theta} = 0$.

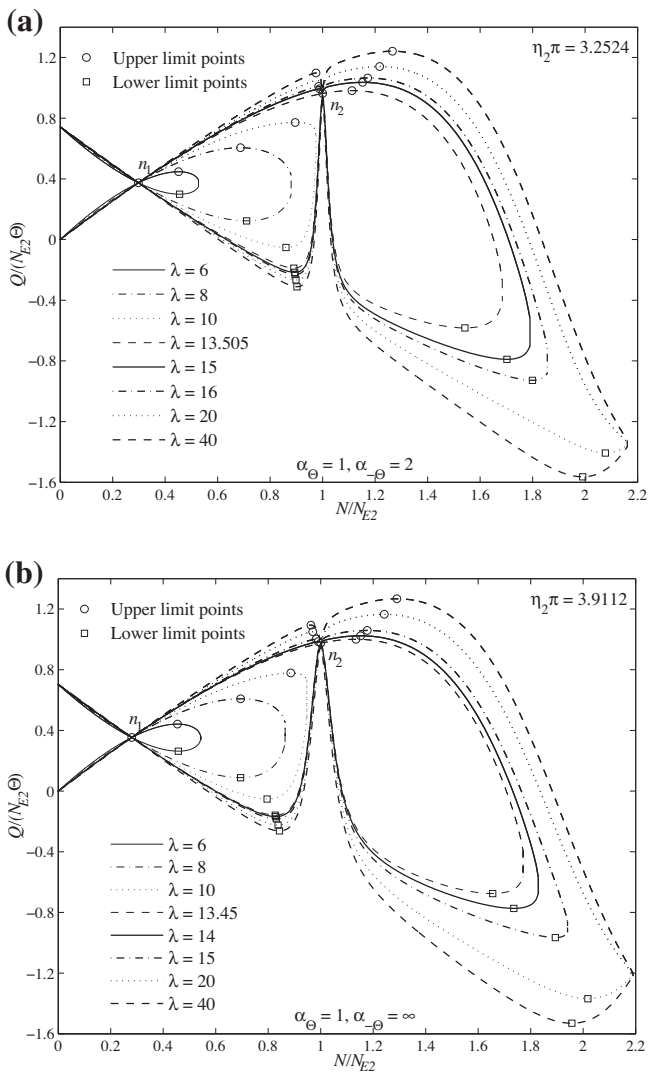

Fig. 7. Non-linear relationship of axial force with central load for arches with $\alpha_\Theta = 1$ and $\alpha_{-\Theta} = 2$ or $\alpha_\Theta = 1$ and $\alpha_{-\Theta} = \infty$.

can be calculated by substituting $\beta = 2.394$ ($\Rightarrow N_{E1}/N_{E2} = 0.3754$) and $P = 3.3638$ ($\Rightarrow Q/(N_{E2}\Theta) = 0.4407$) into Eq. (9) as $v_c/f = 0.899$. The position of the inflection point c in Fig. 4(a) is defined by $N_{E1}/N_{E2} = 0.3754$ and $Q/(N_{E2}\Theta) = 0.4407$.

The specific geometric parameter λ_1 can serve as a switch between arches that have non-linear buckling behaviour and beams curved in elevation that have no typical buckling behaviour. To further illustrate this, variations of the dimensionless axial force N/N_{E2} with the dimensionless load $Q/(N_{E2}\Theta)$ for two groups of arches are shown in Fig. 8(a) for the group with $\alpha_\Theta = 4$ and $\alpha_{-\Theta} = 1$, and in Fig. 8(b) for the group with $\alpha_\Theta = 0.4$ and $\alpha_{-\Theta} = 0.01$. The specific geometric parameter is evaluated as $\lambda_1 = 4.3694$ for the group with $\alpha_\Theta = 4$ and $\alpha_{-\Theta} = 1$, and $\lambda_1 = 7.4195$ for the group with $\alpha_\Theta = 0.4$ and $\alpha_{-\Theta} = 0.01$. It can be seen from Fig. 8(a) that arches with a geometric parameter ($\lambda = 6, 8$ and 10) greater than $\lambda_1 = 4.3694$ have an upper limit point and a lower limit point, while arches with a geometric parameter ($\lambda = 3.5$ and 4) smaller than $\lambda_1 = 4.3694$ have no typical buckling behaviour and so they should be considered as beams curved in elevation. It can also be seen from Fig. 8(b) that arches with a geometric parameter ($\lambda = 9$, 10 and 12) greater than $\lambda_1 = 7.4195$ have an upper limit point and a lower limit point while arches with a geometric parameter ($\lambda = 5$ and 6) smaller than $\lambda_1 = 7.4195$ have no typical buckling behaviour and so they should be considered as beams curved in elevation.

The relative flexibility of the rotational end restraints α_Θ and $\alpha_{-\Theta}$ may also influence the lowest buckling load and the non-linear behaviour. The influences are shown as variations of the dimensionless central radial displacement v_c/f with the dimensionless load $Q/(N_{E2}^{pin}\Theta)$ in Fig. 9(a), and as variations of the dimensionless axial force N/N_{E2}^{pin} with the dimensionless load $Q/(N_{E2}^{pin}\Theta)$ in Fig. 9(b). For the convenience of comparison, the second mode flexural buckling load N_{E2}^{pin} of the pin-ended column with the same length but without rotational end restraints under uniform axial compression is used in Fig. 9(a) and (b) to form the dimensionless load $Q/(N_{E2}^{pin}\Theta)$ and axial force N/N_{E2}^{pin}. It can be seen that for the relative flexibility $\alpha_\Theta = 1$ of the rotational restraint at the end $\theta = \Theta$, as the relative flexibility $\alpha_{-\Theta}$ of the other rotational restraint at the end $\theta = -\Theta$ increases, the dimensionless lowest buckling load and the corresponding dimensionless axial force decrease while the dimensionless central radial displacement at the lowest buckling load increases.

5. Comparisons with finite element results

The analytical solutions for the non-linear behaviour of pin-ended arches with unequal rotational end restraints given by Eqs. (9) and (19) are compared with finite element (FE) predictions

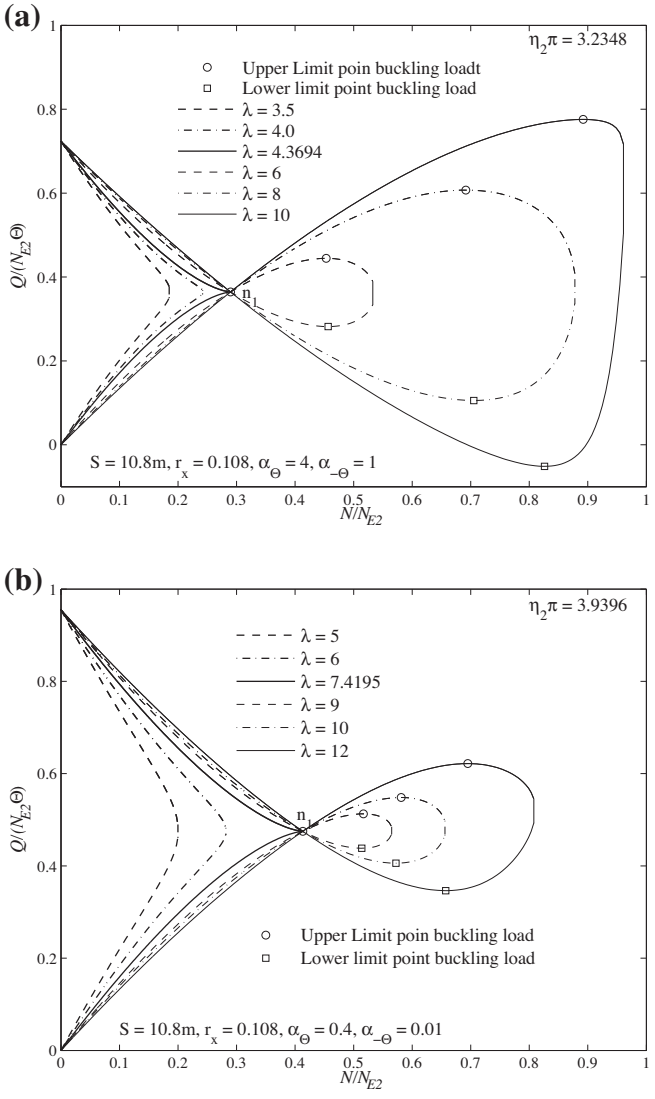

Fig. 8. Non-linear relationship of axial force with central load for arches with $\alpha_\Theta = 4$ and $\alpha_{-\Theta} = 1$ or $\alpha_\Theta = 0.4$ and $\alpha_{-\Theta} = 0.01$.

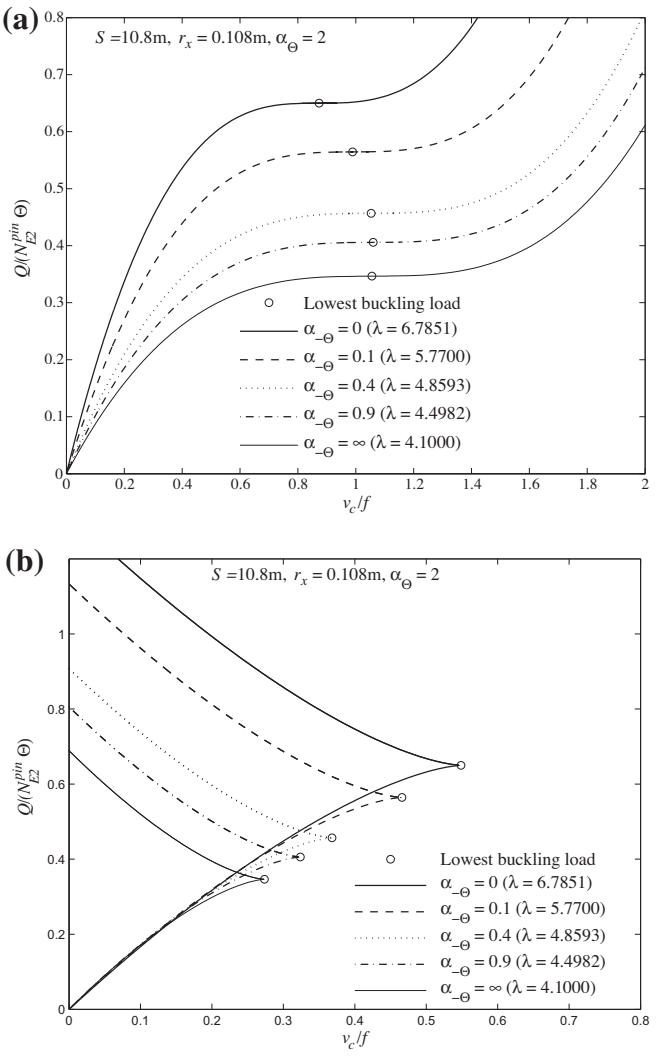

Fig. 9. Effects of flexibility on lowest buckling and postbuckling behaviour.

using the non-linear analysis of ABAQUS (2008) and Pi et al. (2005) in Figs. 10 and 11, as variations of the dimensionless radial load $Q/(N_{E2}\Theta)$ with the dimensionless central radial displacement v_c/f. The arches in Fig. 10 were assumed to have geometric parameters $\lambda = 6$, 10, 15, 20, respectively, and the rotational end restraints of these arches were assumed to have relative flexibilities of $\alpha_\Theta = 1$ and $\alpha_{-\Theta} = 0$. The arches in Fig. 11 were assumed to have the same geometric parameters $\lambda = 15$, with different flexibilities of the rotational end restraints $\alpha_\Theta = 1$ and $\alpha_{-\Theta} = 0.001$, $\alpha_\Theta = 0.1$ and $\alpha_{-\Theta} = \infty$, $\alpha_\Theta = 1$ and $\alpha_{-\Theta} = 0.9$, and $\alpha_\Theta = 1$ and $\alpha_{-\Theta} = \infty$, respectively. In the FE analysis, an I-section was used whose dimensions are: overall depth $D = 0.2613$ m, flange width $B = 0.151$ m, flange thickness $t_f = 0.0123$ m, and web thickness $t_w = 0.0077$ m. The Young's modulus was assumed to be $E = 200{,}000$ MPa. In the ABAQUS FE non-linear analysis, the two dimensional beam element B21 was chosen, 20 elements were used to model the arch, the elastic spring rotational element was used for the rotational end restraints, and the pin-ended conditions were assigned in polar axes. In addition, the non-linear analysis with the global control modified Riks algorithm that is implemented in ABAQUS was used in conjunction with proper load increments and convergence accuracy to obtain the non-linear solutions. When the FE program of Pi et al. (2005) was used, eight curved beam elements were used to model the arches and proper rotational end restraints were assigned. The results of Pi et al. (2005) are identical to those of ABAQUS (2008). It can be seen from Figs. 10 and 11 that the analytical predictions of the non-linear equilibrium paths and buckling loads for arches with different geometric parameters and different rotational end restraints agree very well with their FE counterparts.

6. Conclusions

This paper has studied the non-linear elastic in-plane buckling and postbuckling behaviour of pin-ended shallow circular arches with unequal elastic rotational end restraints under a central concentrated radial load. Analytical solutions for the non-linear in-plane buckling and postbuckling behaviour and for the buckling loads were derived. It was found that the pin-ended arch with elastic rotational end restraints of unequal stiffnesses may buckle in a limit point instability mode, but cannot buckle in a bifurcation mode. It was also shown that the effects of the unequal stiffnesses of the rotational end restraints on the buckling loads and the post-buckling behaviour are significant. The buckling loads increase with a decrease of the relative flexibility (i.e. an increase of the

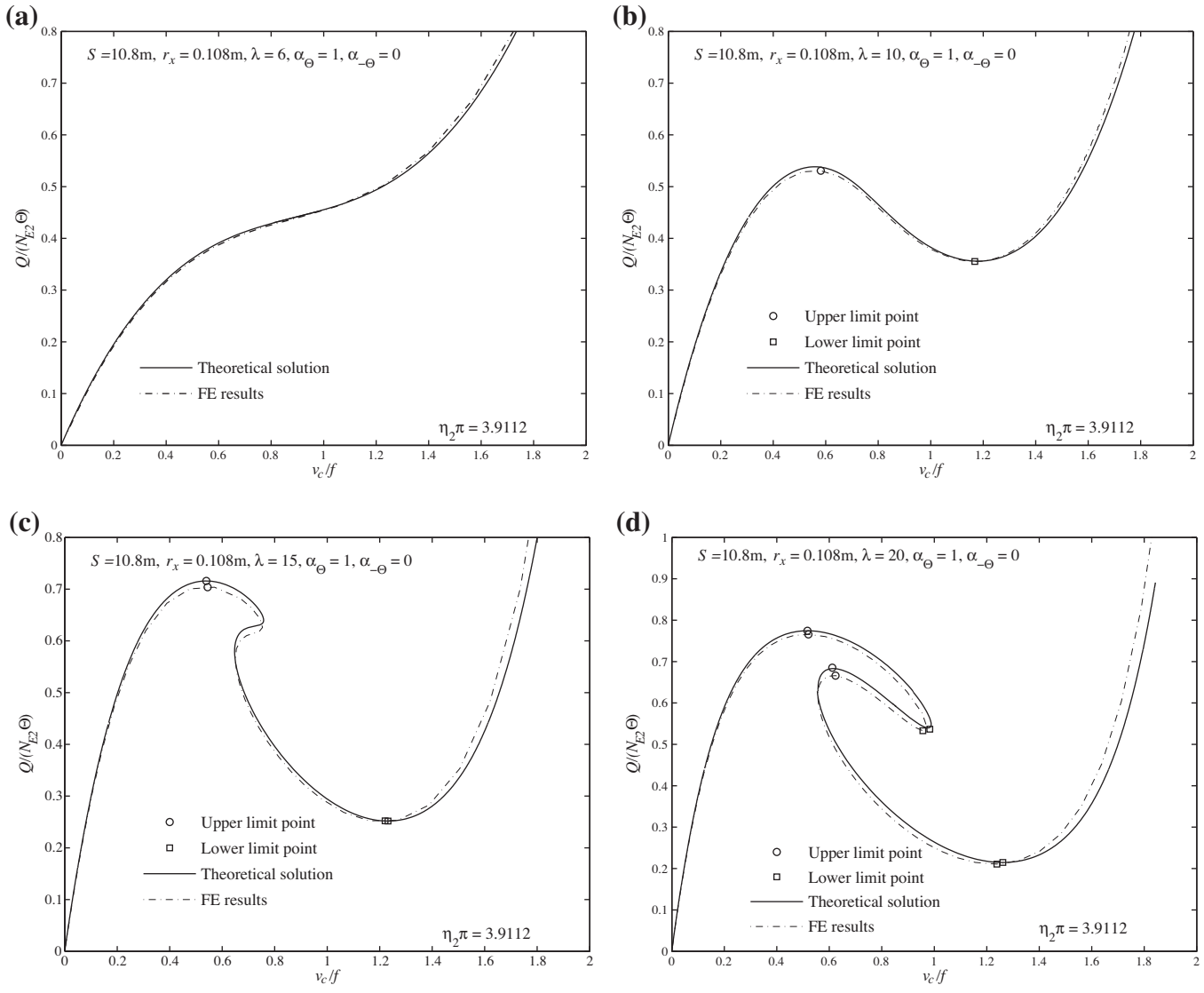

Fig. 10. Comparison of **analytical** solutions with FE results for non-linear behaviour of arches having $\alpha_\Theta = 1$ and $\alpha_{-\Theta} = 0$.

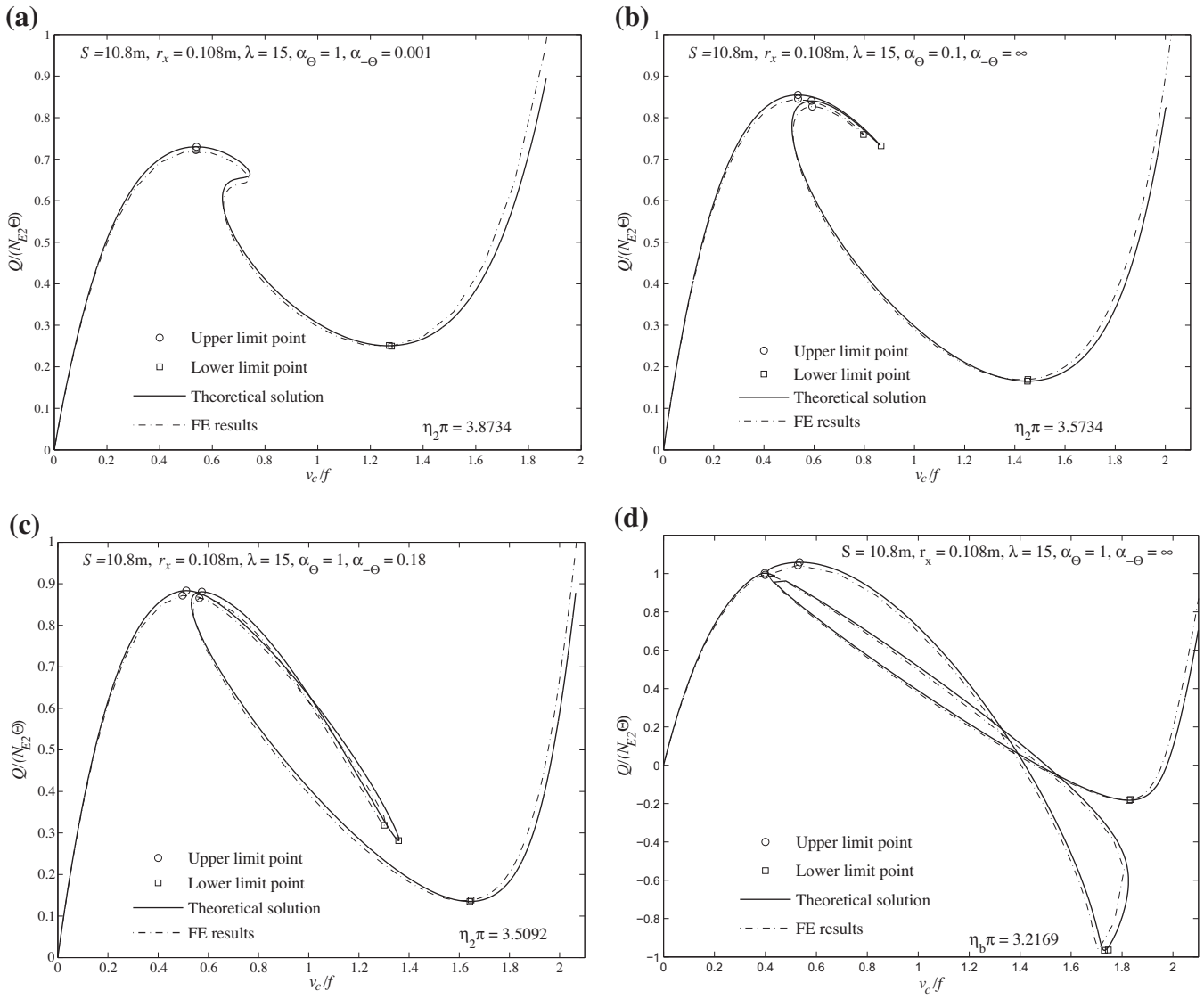

Fig. 11. Comparison of analytical solutions with FE results for non-linear behaviour of arches having $\lambda = 15$.

stiffness) of the elastic rotational end restraints. A specific value of the geometric parameter that defines a switch between arches with an upper limit point and a lower limit point and arches with two upper limit points and two lower limit points was derived. Another specific value of the geometric parameter that defines a switch between arches and beams curved in elevation was derived. Comparisons with the FE predictions have shown that the analytical solutions derived in this paper can accurately predict the non-linear behaviour and buckling loads of shallow arches with unequal end rotational restraints.

Acknowledgements

This work has been supported by the Australian Research Council through Discovery Projects (DP1097096 and DP1096454) awarded to both authors and an Australian Laureate Fellowship (FL100100063) awarded to the second author.

References

ABAQUS, 2008. Theory Manual, Version 6.7. Hibbit. Karlsson and Sorensen Inc., Pawtuchet, RI.

Bažant, Z.P., Cedolin, L., 2003. Stability of Structures. Dover Publications Inc., Minneola, NY.

Bradford, M.A., Uy, B., Pi, Y.-L., 2002. In-plane stability of arches under a central concentrated load. Journal of Engineering Mechanics ASCE 128 (7), 710–719.

Dickie, F.F., Broughton, P., 1971. Stability criteria for shallow arches. Journal of the Engineering Mechanics Division ASCE 97 (EM3), 951–965.

Gjelsvik, A., Bodner, S.R., 1962. Energy criterion and snap-through buckling of arches. Journal of the Engineering Mechanics Division ASCE 88 (EM5), 87–134.

Hodges, D.H., 1999. Non-linear in-plane deformation and buckling of rings and high arches. International Journal of Non-Linear Mechanics 34 (4), 723–737.

Kyriakides, S., Arseculeratne, R., 1993. Propagating instabilities in long shallow panels. Journal of Engineering Mechanics ASCE 119 (3), 570–583.

Pi, Y.-L., Bradford, M.A., Uy, B., 2002. In-plane stability of arches. International Journal of Solids and Structures 39 (1), 105–125.

Pi, Y.-L., Bradford, M.A., Uy, B., 2005. A spatially curved-beam element with warping and Wagner effects. International Journal for Numerical Methods in Engineering 63, 1342–1369.

Pi, Y.-L., Bradford, M.A., Tin-Loi, F., 2007. Nonlinear analysis and buckling of elastically supported circular shallow arches. International Journal of Solids and Structures 44, 2401–2425.

Pi, Y.-L., Bradford, M.A., Tin-Loi, F., 2008. Nonlinear in-plane buckling of rotationally restrained shallow arches under a central concentrated load. International Journal of Non-Linear Mechanics 43 (1), 1–17.

Pi, Y.-L., Bradford, M.A., 2009. Non-linear in-plane postbuckling of arches with rotational end restraints under uniform radial loading. International Journal of Non-Linear Mechanics 44 (9), 975–989.

Pi, Y.-L., Bradford, M.A., 2010. Effects of prebuckling analysis on determining buckling loads of pin-ended circular arches. Mechanics Research Communications 37, 545–553.

Pi, Y.-L., Bradford, M.A., 2012. Non-linear in-plane analysis and buckling of pinned-fixed shallow arches subjected to a central concentrated load. International Journal of Non-Linear Mechanics 47 (1), 118–131.

Power, T.L., Kyriakides, S., 1994. Localization and propagation of instabilities in long shallow panels under external pressure. Journal of Applied Mechanics ASME 61 (4), 755–763.

Schreyer, H.L., Masur, E.F., 1966. Buckling of shallow arches. Journal of the Engineering Mechanics Division ASCE 92 (EM4), 1–17.

Simitses, G.J., 1976. An Introduction to the Elastic Stability of Structures. Prentice-Hall, Englewood Cliffs, NJ.

Simitses, G.J., Hodges, D.H., 2006. Fundamentals of Structural Stability. Elsevier, Boston.

Timoshenko, S., Gere, J.M., 1961. Theory of Elastic Stability. McGraw-Hill Co. Inc., New York.